Delft University of Technology

Modeling and Characterization of Pre-Charged Collapse-Mode CMUTs

Saccher, Marta; Kawasaki, Shinnosuke ; Klootwijk, Johan; van Schaijk, Rob; Dekker, Ronald

DOI
10.1109/OJUFFC.2023.3240699

Publication date
2023

Document Version
Final published version

Published in
IEEE Open Journal of Ultrasonics, Ferroelectrics, and Frequency Control

Citation (APA)
Saccher, M., Kawasaki, S., Klootwijk, J., van Schaijk, R., & Dekker, R. (2023). Modeling and Characterization of Pre-Charged Collapse-Mode CMUTs. *IEEE Open Journal of Ultrasonics, Ferroelectrics, and Frequency Control*, *3*, 14-28. https://doi.org/10.1109/OJUFFC.2023.3240699

Important note
To cite this publication, please use the final published version (if applicable).
Please check the document version above.

Copyright
Other than for strictly personal use, it is not permitted to download, forward or distribute the text or part of it, without the consent of the author(s) and/or copyright holder(s), unless the work is under an open content license such as Creative Commons.

Takedown policy
Please contact us and provide details if you believe this document breaches copyrights.
We will remove access to the work immediately and investigate your claim.

This work is downloaded from Delft University of Technology.
For technical reasons the number of authors shown on this cover page is limited to a maximum of 10.

IEEE Open Journal of Ultrasonics, Ferroelectrics, and Frequency Control

Received 30 November 2022; revised 13 January 2023; accepted 25 January 2023.
Date of publication 30 January 2023; date of current version 16 February 2023.

Digital Object Identifier 10.1109/OJUFFC.2023.3240699

Modeling and Characterization of Pre-Charged Collapse-Mode CMUTs

MARTA SACCHER[1] (Graduate Student Member, IEEE), SHINNOSUKE KAWASAKI[1], JOHAN H. KLOOTWIJK[2] (Senior Member, IEEE), ROB VAN SCHAIJK[3], AND RONALD DEKKER[1,3]

[1]Microelectronics Department, Delft University of Technology, 2628 CT Delft, The Netherlands
[2]Philips Research, 5656 AE Eindhoven, The Netherlands
[3]Philips Engineering Solutions, 5656 AE Eindhoven, The Netherlands

CORRESPONDING AUTHOR: M. SACCHER (M.Saccher@tudelft.nl)

This work was supported in part by the Electronic Components and Systems for European Leadership (ECSEL) Joint Undertaking Project Moore4Medical under Grant H2020-ECSEL-2019IA-876190 and in part by the ULIMPIA Project which is a labeled PENTA Project endorsed by EUREKA under PENTA Cluster under Grant E!9911.

This article has supplementary downloadable material available at https://doi.org/10.1109/OJUFFC.2023.3240699, provided by the authors.

ABSTRACT Recently, the applications of ultrasound transducers expanded from high-end diagnostic tools to point of care diagnostic devices and wireless power receivers for implantable devices. These new applications additionally require that the transducer technology must comply to biocompatibility and manufacturing scalability. In this respect, Capacitive Micromachined Ultrasound Transducers (CMUTs) have a strong advantage compared to the conventional PZT based transducers. However, current CMUTs require a large DC bias voltage for their operation, which limits the miniaturizability of these devices. In this study, we propose a pre-charged collapse-mode CMUT for immersive applications that can operate without an external bias by means of a charge trapping Al_2O_3 layer embedded in the dielectrics between the top and bottom electrodes. The built-in charge layer was analytically modeled and four layer stack combinations were investigated and characterized. The measurement results of the CMUTs were then used to fit the model and to quantify the amount and type of trapped charge. It was found that these devices polarize due to the ferroelectric-like behavior of the Al_2O_3, and the amount of charge stored in the charge-trapping layer was estimated to be approximately 0.02 C/m^2. Their acoustic performance shows a transmit and receive sensitivity of 8.8 kPa/V and 13.1 V/MPa respectively. In addition, we show that increasing the charging temperature, the charging duration, and the charging voltage results in a higher amount of stored charge. Finally, results of ALT tests showed that these devices have a lifetime of more than 2.5 years at body temperature.

INDEX TERMS CMUT, zero-bias CMUTs, collapse-mode CMUTs, ultrasound transducer.

I. INTRODUCTION

VISUALIZING the inside of the body by using ultrasound has mainly been limited to the hospital environment over the last three to four decades [1]. These hospital environments required high-quality ultrasound systems to make accurate diagnoses, leading to drastically improved performance of the ultrasound equipment [2]. However, in recent years, there has been an emerging low-end ultrasound market that accommodates new customer/patient demands, such as using ultrasound to continuously monitor the status of various visceral organs (i.e., heart, bladder), or as a handheld ultrasound system that can be connected to a smartphone to make on-site visualization in resource-limited settings [3], [4]. Furthermore, ultrasound transducers are expanding their application from a diagnostic tool to wireless power receivers that can be used within the human body to power the next generation of implantable devices [5], [6], [7]. The requirements for these new applications are different compared to the traditional high-end diagnostic ultrasound market, which solely focused on image quality, and not on challenges such as connectivity to the internet, portability, lower price, biocompatibility, and manufacturing scalability to name a few. However, the current manufacturing processes based on lead zirconate titanate (PZT) ultrasound transducer devices do not meet these requirements. Limitations include the inherent labor cost associated with the manual assembly of PZT

This work is licensed under a Creative Commons Attribution 4.0 License. For more information, see https://creativecommons.org/licenses/by/4.0/

transducers or the use of toxic metals (lead), which limits in-body use.

Alternatively, micromachined ultrasonic transducers (MUTs) can be used and made biocompatible. MUTs have a suspended membrane over a vacuum gap, and through the vibration of this membrane, ultrasound can be transmitted into, or received from the medium interfacing the membrane. Due to this thin membrane structure, MUTs have a broader bandwidth compared to conventional PZT transducers. MUTs are fabricated through standard IC-based fabrication processes, making them CMOS compatible, enabling mass production and simple integration with peripheral electronics at a lower cost. Depending on the actuation mechanism, MUTs can be categorized either as CMUTs (Capacitive Micromachined Ultrasound Transducers) or PMUTs (Piezoelectric Micromachined Ultrasound Transducers). CMUTs are actuated electrostatically with an opposing electrode beneath the vacuum gap. Alternatively, PMUTs are actuated with a thin-film piezoelectric material embedded within the top membrane.

Comparing these two technologies, CMUT technology has matured to the level that they are now used in commercially available point of care applications [4]. In addition, a recent benchmark of the performance parameters of CMUTs and PMUTs executed by European companies and institutes showed that CMUTs have the best overall acoustical performance, with higher receive and transmit sensitivity than most of the PMUT devices [8]. Typical values of receive sensitivity for CMUTs range between 2.5 and 10 V MPa^{-1} and transmit sensitivity ranges from 4 to 23 kPa V^{-1}. The downside of using CMUTs is the (large) DC bias voltage required for their operation. Typically, around 50 V to 100 V is needed to bring the top membrane closer (non-collapse mode) or in contact (collapse-mode) to the bottom membrane to increase the electric field strength, which increases the sensitivity of these devices. This leads to three undesired consequences. In the first place, the high DC voltage source requires additional board space limiting the portability/miniaturizability of these devices. Secondly, the reliability of individual transducers is coupled to other transducers since one shorting element will inadvertently affect the DC bias voltage connected to the other elements and thirdly, large bias voltages are not desirable for medical applications, where patient safety is of paramount importance.

In this work, we propose a pre-charged collapse-mode CMUT for in-body applications that can operate without an external bias voltage and where there is sufficient built-in charge to keep the CMUT in collapse-mode. To accomplish this, we use the dielectric charging behavior of Al_2O_3. Dielectric charging is usually seen as a reliability issue in MEMS devices since it causes instability of the device characteristics up to the point at which the device fails [9], [10], [11]. On the other hand, the concept of dielectric charging is at the base of the semiconductor memory industry [12], [13], [14], and other groups have already experimentally applied it to CMUT devices to achieve reduced or zero-bias operation [15], [16], [17], [18], [19]. High-k materials such as Si_3N_4 or HfO_2 could be used for this application [20], as investigated by Park et al. [18] and Choi et al. [15], who demonstrated the feasibility of pre-charged CMUTs with Si_3N_4 as dielectric showing good charge retention over time, even at high temperatures. Charge retention over time represents the major challenge for these devices and, depending on the application, the minimum lifetime can vary from hours in the case they are part of a disposable device, or a few months for acute applications, to years. Most of the studies concerning pre-charged CMUTs investigated non-collapse mode operation since the amount of charge stored in the device was not enough to keep the membrane in contact with the bottom membrane. This depends on the material of the dielectric layer, the deposition method and the structure of the device. To the authors knowledge, only one pre-charged collapse-mode device has been published in literature [17], however operating at low frequency (140 kHz) and without reporting the acoustic performance and lifetime.

The aim of this paper is to show that it is possible to obtain pre-charged collapse-mode CMUTs using Al_2O_3 as charge trapping layer, and to present a comprehensive analysis of the device characteristics and performance through modeling and measurements. The remainder of this paper is organized as follows: the first section introduces a model of the pre-charged CMUT which is an extension of the work presented by Koymen et al. [21] where a CMUT was modeled assuming two types of built-in charges: surface charge of the opposite polarity at both sides of the charging layer forming an electret, and spatially fixed volume charge uniformly distributed within the charging layer. In the second section, four CMUT devices, each with a different layer stack are introduced. A description of the methods used to characterize the devices and fit the model are presented, followed by their results in the next section. It is shown that this model well describes the characteristics of the four CMUTs and that it can be used to estimate the type and amount of built-in charges. In the third section, the performance of the pre-charged devices in terms of transmit and receive sensitivity, and output pressure is evaluated. In addition, the effect of different charging parameters (e.g. charging temperature, charging voltage and polarity, and charging duration) on the amount of charge stored in the CMUTs is studied, resulting in a general relationship. The final part of this section presents the estimated lifetime of these devices obtained from charge retention studies by means of accelerated lifetime tests.

II. MODELING THE PRE-CHARGED CMUT

This section introduces a theoretical model of the collapse-mode CMUTs with a built-in charge layer. A schematic representation of the pre-charged collapse-mode CMUT is shown in Fig. 1 (a). In this model, the CMUT is modeled as a vibrating axisymmetric clamped membrane. The charging layer is embedded between the top and bottom

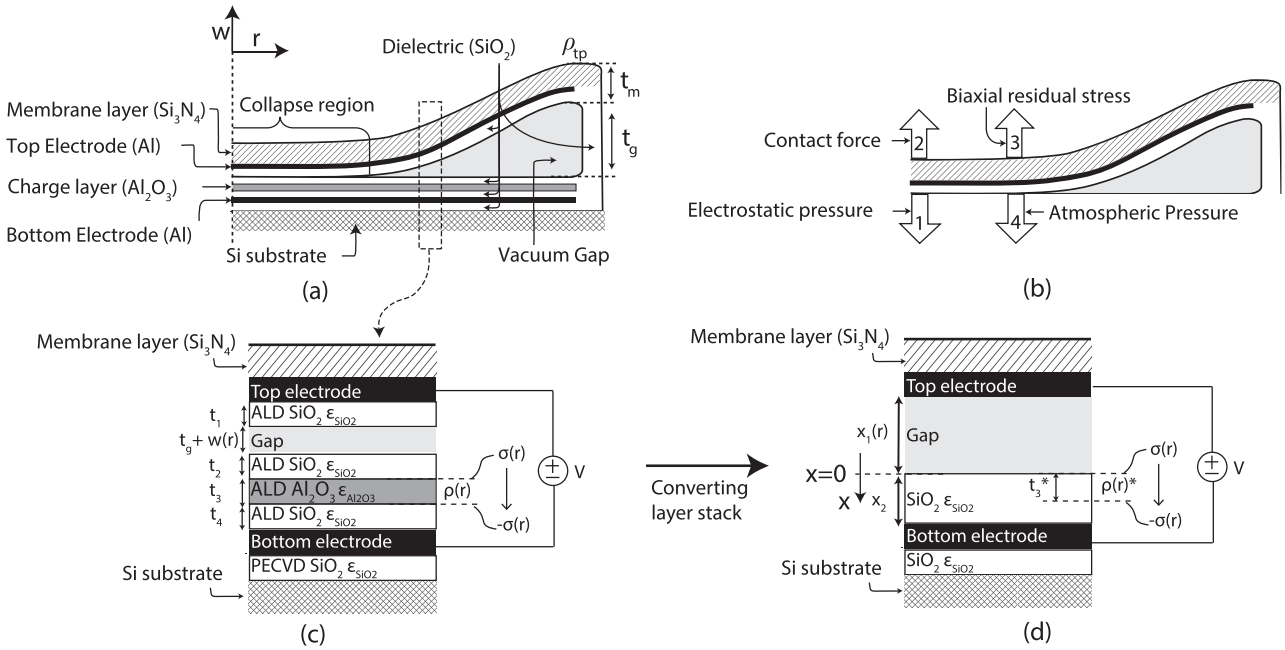

FIGURE 1. (a) Cross section of the CMUT. (b) Forces acting on the top membrane. (c) Expanded view of the CMUT layer stack. (d) Converted layer stack.

electrodes, separated by an insulation layer. In Fig. 1(a), t_m is the thickness of the top membrane, which includes the SiO_2 dielectric layer, the top electrode and the Si_3N_4 membrane layer. ρ_{tp} is the mass density of the top membrane, t_g is the height of the vacuum gap and $w(r)$ is the displacement of the membrane along the radial direction r. The voltage V is defined with respect to the bottom electrode as in the remainder of this paper. Fig. 1(b) denotes the forces acting on the top membrane which are 1) the electrostatic pressure resulting from the built-in charge and the external voltage, 2) the contact force which is the reactive force that occurs where the top membrane touches the bottom membrane, 3) the uniform biaxial residual stress and 4) the atmospheric pressure.

According to [22], the governing dynamic equation without the built-in charge is given by:

$$\rho_{tp} t_m \frac{\partial^2 w(r,t)}{\partial^2 t} + D\nabla_r^4 w(r,t) = -\frac{\varepsilon_0}{2(t_{eff}+w(r,t))^2}V(t)^2 + \frac{H_{ab}}{2}\mathrm{erfc}\left(\frac{t_g + w(r,t)}{\sigma_m\sqrt{\pi}}\right) + \frac{\tau t_m}{r}\frac{\partial}{\partial r}\left(r\frac{\partial w(r)}{\partial r}\right) - P_{atmos} \quad (1)$$

$$\nabla_r^4 = \left(\frac{\partial^2}{\partial r^2} + \frac{1}{r}\frac{\partial}{\partial r}\right)^2. \quad (2)$$

The four terms on the right side of (1) correspond to the four different forces previously mentioned. Furthermore, D is the flexural rigidity of the top membrane, $V(t)$ is the external voltage applied to the top membrane, σ_m is the standard deviation of the combined surface roughnesses, H_{ab} is the indentation hardness, τ is the uniform biaxial residual stress, erfc is the complementary error function, and t_{eff} is the effective gap height between the top and bottom electrode corrected for the dielectric constants, which is defined as:

$$t_{eff} = t_g + \sum \frac{t_i}{\varepsilon_i}, \quad (3)$$

where t_i, is the thickness of the dielectric layers between the top and bottom electrodes divided by their corresponding dielectric constants. For further details, readers are referred to [22]. In this work, (1) was adapted by adding the electrostatic force from the built-in charge.

Fig. 1(c) is a cross-section of the CMUT at an arbitrary radius r. In this figure, the dielectric layer thickness is denoted as t with a subscript from 1 to 4. The charge trapping layer has a dielectric constant of $\varepsilon_{Al_2O_3}$ and is sandwiched between two SiO_2 layers. The charge distribution within the charge trapping layer is defined by a homogeneous charge of $\rho(r)$ [$\mathrm{C\,m^{-3}}$] inside the charging layer, as well as a downwards polarization induced by a surface charge of $\sigma(r)$ [$\mathrm{C\,m^{-2}}$] with opposite polarities on both sides of the charging layer.

Due to the multiple dielectric constants used in this layer stack, there is no simple solution that can be directly used to calculate the electrostatic force. However, for a simpler model as the one shown in Fig. 1(d), where there is only one dielectric layer on one side of the electrode, and the other side is a vacuum gap, Sessler [23] derived the electrostatic pressure on the top electrode for a generalized charge distribution within the dielectric layer. Thus, the electrostatic force on the top membrane can be derived by converting the layer stack and

the charge distribution of Fig. 1(c) to Fig. 1(d). By comparing Fig. 1(c) to Fig. 1(d) we see that:

$$x_1(r) = \mathrm{t_g} + w(r) + \frac{\mathrm{t_1} + \mathrm{t_2}}{\varepsilon_{SiO_2}}$$
$$\mathrm{x_2} = \mathrm{t_4} + \mathrm{t_3}\frac{\varepsilon_{SiO_2}}{\varepsilon_{Al_2O_3}}. \tag{4}$$

In these two equations, $\mathrm{t_1}$, $\mathrm{t_g} + w(r)$ and $\mathrm{t_2}$ are converted to $x_1(r)$ which has a relative permittivity of vacuum and $\mathrm{t_3}$, $\mathrm{t_4}$ are converted to $\mathrm{x_2}$ which has a relative permittivity of SiO_2. For convenience, we denote $\mathrm{t_3^*} = \mathrm{t_3}\frac{\varepsilon_{SiO_2}}{\varepsilon_{Al_2O_3}}$ in the following derivation. Since the total amount of charge should not change, the charge distribution is scaled as $\rho^*(r) = \rho(r)\frac{\varepsilon_{Al_2O_3}}{\varepsilon_{SiO_2}}$ so that $\rho^*(r)\mathrm{t_3}^* = \rho(r)\mathrm{t_3}$. As a result, the charge distribution for the equivalent layer stack is:

$$\rho^*(r, x) = \begin{cases} \sigma(r)\delta(x) - \sigma(r)\delta(x - \mathrm{t_3^*}) + \rho^*(r), & \text{if } 0 \le x \le \mathrm{t_3^*} \\ 0 & \text{otherwise} \end{cases} \tag{5}$$

where $\delta(x)$ is a dirac delta function used to express the surface charge density. Referring to [23] (eq. 14 and eq. 34), the electrostatic pressure acting on the top membrane for a generalized charge distribution is:

$$P_e(r) = -\frac{\varepsilon_0}{2s(r)^2}\left(\mathrm{V} - V_{eff}(r)\right)^2 \tag{6}$$

where

$$V_{eff}(r) = \frac{\mathrm{x_2}\sigma_1(r)}{\varepsilon_0\varepsilon_{SiO_2}} \tag{7}$$
$$s(r) = \mathrm{t_{eff}} + w(r) \tag{8}$$

and

$$\sigma_1(r) = \frac{1}{\mathrm{x_2}}\int_0^{\mathrm{x_2}}(\mathrm{x_2} - x)\rho^*(r, x)\,dx. \tag{9}$$

From (6), the force from the internal charge acts effectively as if a voltage of $V_{eff}(r)$ is subtracted from the external voltage V. The only unknown value in this equation is $\sigma_1(r)$, which is the contribution of the surface and the volume charges. By inserting (5) into (9) and integrating, we find:

$$\sigma_1(r) = \mathrm{t_3}\left(1 - \frac{\mathrm{t_3^*}}{2\mathrm{x_2}}\right)\rho(r) + \frac{\mathrm{t_3}^*}{\mathrm{x_2}}\sigma(r). \tag{10}$$

From this result, $\sigma_1(r)$ is characterized as the sum of the volume charge (1st term) and the surface charge (2nd term). Finally, we include the modified electrostatic pressure by including the internal charge (6) into the membrane dynamics (1) as:

$$\rho_{\mathrm{tp}}\mathrm{t_m}\frac{\partial^2 w(r,t)}{\partial^2 t} + \mathrm{D}\nabla_r^4 w(r,t) = -\frac{\varepsilon_0}{2(\mathrm{t_{eff}} + w(r,t))^2}\left(V(t) - V_{eff}(r)\right)^2 + \frac{\mathrm{H_{ab}}}{2}\mathrm{erfc}\left(\frac{\mathrm{t_g} + w(r,t)}{\sigma_m\sqrt{\pi}}\right) + \frac{\tau\mathrm{t_m}}{r}\frac{\partial}{\partial r}\left(r\frac{\partial w(r)}{\partial r}\right) - \mathrm{P_{atmos}}. \tag{11}$$

The above equation can be numerically solved by non-dimensionalizing the equation and using the Galerkin Approach with six or more vibrational modes, which was found to be sufficient in prior work [24], [25]. Finally, this equation can be extended to CMUT operation in water if mutual and self-acoustic loading are incorporated. However, for the scope of this work this was not taken into account. All the variables used in this work are summarized in Appendix, Table 2.

A. CHARGE DISTRIBUTION

In this work, charges are injected into the charging layer by applying a bias voltage to bring the CMUT into collapse mode and by tunneling charges through the circular region where the top and bottom membranes are in contact. Consequently, the injected charges will have an axial symmetric distribution. In this work, for simplicity, the charge distribution was defined by a homogeneous distribution immediately beneath the contact area. The following equation mathematically expresses this distribution along the radius of the CMUT for the surface charge $\sigma(r)$ and volumetric charge $\rho(r)$ as:

$$\sigma(r) = \begin{cases} \sigma_0, & \text{for } 0 \le r \le r_{charge} \\ 0 & \text{for } r_{charge} < r \le \mathrm{a} \end{cases} \tag{12}$$

$$\rho(r) = \begin{cases} \rho_0, & \text{for } 0 \le r \le r_{charge} \\ 0 & \text{for } r_{charge} < r \le \mathrm{a} \end{cases} \tag{13}$$

where, r_{charge} is the contact radius during the charging process, a is the radius of the CMUT, σ_0 and ρ_0 are constants for the surface charge density and the volumetric charge density beneath the contact region after charging.

B. QUALITATIVE CHANGES IN THE C-V CURVE

When different types of charges are trapped inside a CMUT, the Capacitance to Voltage (C-V) curve shifts with respect to the 0 V axis. The root cause can be seen in (6), where there is a second term $V_{eff}(r)$ that is subtracted from the external voltage V. In the previous section it was defined that charges will be distributed only between $0 < r < r_{charge}$. Thus, for $r_{charge} > 0$, $V_{eff}(r) = 0$ from (7,10).

In this section we qualitatively describe in which direction the C-V curve will shift depending on the charge that is distributed between $0 < r < r_{charge}$ of the CMUT. If $V_{eff}(r) > 0$, the internal voltage acts against the external voltage V, thus requiring a larger voltage to bring the CMUT into collapse, which will shift the C-V curve to the right. If $V_{eff}(r) < 0$ the internal voltage acts alongside the external voltage V shifting the C-V curve to the left. Therefore, the sign of $V_{eff}(r)$ indicates in which direction the C-V curve will shift. In this section, the following four cases are considered, and the actual charging can be considered as a combination of these four cases:

Case 1 ($\sigma_0 = 0$, $\rho_0 < 0$)**:** Only electrons.
Case 2 ($\sigma_0 > 0$, $\rho_0 = 0$)**:** Only downward polarization.
Case 3 ($\sigma_0 < 0$, $\rho_0 = 0$)**:** Only upward polarization.
Case 4 ($\sigma_0 = 0$, $\rho_0 > 0$)**:** Only holes.

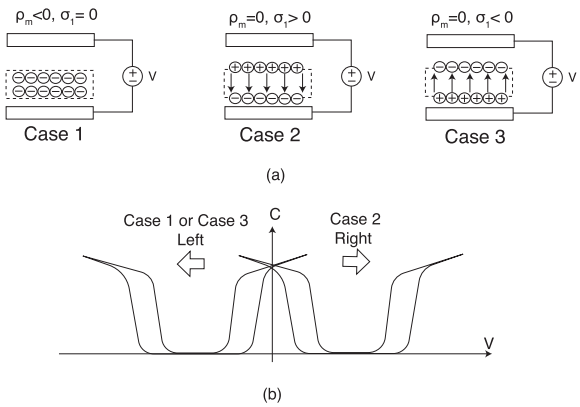

FIGURE 2. (a) A schematic drawing of where and which polarity of charge is trapped for the three cases. (b) Shift in C-V curve: Case 1 and Case 3 the C-V curve will shift to the left; Case 2 the C-V curve will shift to the right.

Case 4 is also included in the list, yet it is unlikely that this situation will arise given that the dielectric stack is sandwiched in between two metal conductors where no injection of holes exist. Thus, we will examine the three other cases in more detail and how they will shift the C-V curve. Fig. 2(a) shows a cartoon drawing of how the charges are positioned in the dielectric layer for the three cases. The sign of V_{eff} is equivalent to finding the sign of σ_1 according to (7) and the definition of σ_1 can be found in (10). Since the coefficients multiplied to the $\rho(r)$ and $\sigma(r)$ are both positive, the sign of V_{eff} can be easily found for each case as, Case 1 and Case 3: $V_{eff} < 0$ ($\because \sigma_1 < 0$) and for Case 2: $V_{eff} > 0$ ($\because \sigma_1 > 0$). Thus the C-V curve will shift to the left for Case 1 and 3 and will shift to the right in Case 2 as shown in Fig. 2(b).

The magnitude of trapped charge is typically derived through measuring how much the C-V curve is shifted. However, if different types of charges are superimposed, this method does not work. For our work we derive the amount of trapped charge by comparing the measured C-V profile with the modelled C-V profile.

III. MATERIALS AND METHODS

A. FOUR CMUT DESIGN VARIANTS AND TEST CAPACITORS

The CMUT cells used in this work have been fabricated using a standard sacrificial release processing. The transducer stack consists of a silicon wafer covered with SiO_2 for insulation, a bottom electrode insulated with a stack of ALD deposited $SiO_2/Al_2O_3/SiO_2$, a vacuum cavity created by wet etching a sacrificial layer made of Al, an ALD SiO_2, a top metal electrode covered with SiO_2, and a Si_3N_4 membrane layer on top (Fig. 1(c)). More information on the fabrication process of the CMUT can be found in [26].

The diameter of the CMUT membrane is 135 µm and a single CMUT element consists of 56 CMUT cells connected in parallel. Four CMUT layer stack combinations were tested to find the optimal layer stack for charge retention, each having slightly different thicknesses for the insulation layer, charge trapping layer, and the vacuum gap. The four variants (A, B, C, and D) used for this work are summarized in Table 1. Despite the similarities, a closer look at the layer stack combinations shows that these devices have many differences making a one-to-one comparison impossible. Such parameter variations are not ideal for a comparative study such as this one, however these devices were initially fabricated to understand the use of high-k materials to achieve a higher acoustic output pressure. Yet, upon their operation, these devices showed charging of the dielectric. This phenomenon was not observed for previous devices manufactured with only SiO_2 as the dielectric and with the same fabrication process.

In addition, to characterize the charging behavior of the CMUTs, test capacitors with an area of 200 µm × 200 µm were fabricated following the same processing steps as the CMUTs, but without depositing the sacrificial layer (Fig. 3(b)).

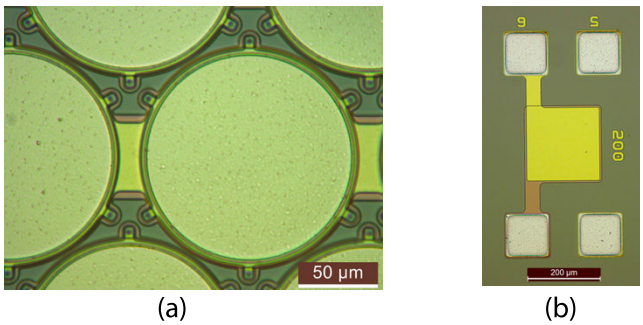

FIGURE 3. Microscope view of (a) a CMUT cell and (b) a test capacitor.

B. CHARACTERIZATION METHODS FOR THE CMUTs AND TEST CAPACITORS

The test capacitors were characterized by measuring the current-voltage (I-V) curve using a Keithley 237 High Voltage Source Measure Unit. Using this instrument, first a linear voltage sweep was used to determine the breakdown voltage of a pristine test capacitor, where pristine indicates a device that has never been tested or used. The voltage was swept between 0 V and 350 V with a hold period of 1 ms at each voltage step and a compliance current of 1 mA. A second linear sweep was then applied to another pristine capacitor with the same layer stack from 0 V to slightly before the breakdown voltage, with a hold period of 1 ms and a voltage step between 0.4 V and 0.6 V, depending on the maximum voltage of the sweep and being limited by the maximum number of measurement points of the instrument.

The CMUT devices were characterized by measuring the membrane profile with a Digital Holographic

TABLE 1. Simulation parameters.

	A	B	C	D	Unit	Description
t_1	0	30	50	75	nm	Insulation thickness see Fig. 1(c)
t_2	50	30	50	75	nm	Insulation thickness see Fig. 1(c)
t_3	200	240	200	250	nm	Charge layer thickness see Fig. 1(c)
t_4	50	10	50	50	nm	Insulation layer thickness see Fig. 1(c)
t_{eff}	546	544	558	474	nm	Total effective thickness (3)
EOT	190	190	240	300	nm	Effective oxide thickness*
t_m	2500	2500	3000	3100	nm	Total thickness of the top membrane
t_g	500	500	500	400	nm	Gap height
D	$2.4{\cdot}10^{-7}$	$2.4{\cdot}10^{-7}$	$4.1{\cdot}10^{-7}$	$4.5{\cdot}10^{-7}$	$Pa \cdot m^3$	Flexural rigidity
ρ_{tp}	3290	3290	3290	3290	$kg \cdot m^{-3}$	Combined mass density of the top plate
a	67.5				µm	Plate Radius
ε_0	$8.85{\cdot}10^{-12}$				$F \cdot m^{-1}$	Vacuum Permittivity
ε_{SiO_2}	4.3				-	Relative Permittivity of SiO_2
$\varepsilon_{Al_2O_3}$	8.8				-	Relative Permittivity of Al_2O_3
P_{atmos}	$1.01325 \cdot 10^5$				Pa	Atmospheric pressure
H_{ab}, n = a, b	$2{\cdot}10^9$				Pa	Indentation hardness
σ	4				nm	Combined surface roughness standard deviation
modes	6				-	Number of vibrational modes used

* $EOT = t_1 + t_2 + t_4 + t_3 \cdot \frac{\varepsilon_{SiO_2}}{\varepsilon_{Al_2O_3}}$

Microscope (DHM) and Capacitance-Voltage (C-V) curves for charged and uncharged devices. Digital Holographic Microscopy (DHM) is a non-contact method used to characterize 3D topography, providing real-time images of the sample profile. In this work, a DHM system (LynceeTec, Switzerland) was used to characterize the membrane profile of the CMUT elements at different externally applied DC bias voltages. C-V curves were obtained with a fast C-V protocol which allows for the measurement of the pull-in and snap-out voltages of the CMUT, minimizing the alteration of the amount of stored charge. For the C-V measurement, a small AC signal at 125 MHz was superimposed on a 200 Hz triangular wave varying between 0 V and ±120 V. The change in the phase of the impedance when the CMUT goes in and out of collapse is used to draw the C-V curve. Two measurement protocols were used: a DC bipolar sweep between positive and negative voltages, and a DC unipolar sweep for either only positive or negative voltages.

C. PRE-CHARGING THE CMUTs

Pristine CMUT elements were pre-charged at room temperature using a programmable source meter (Keithley 2450). The same parameters were used for all four devices to compare their charging capabilities. Other groups that investigated pre-charged CMUTs, charged their devices with voltages between 1.5 to 2.5 times the pull-in voltage [15], [16], [17], [18], [19], mostly resulting, except for one case [17], in out of collapse pre-charged CMUTs. In this work, the amplitude of the DC charging voltage was chosen to be about three times higher than the analytically calculated pull-in voltage out of the four devices, in order to initiate charge trapping in a deep collapsed state. The pull-in voltage V_{pi} was calculated using the equation derived using the parallel plate theory [27]:

$$V_{pi} \simeq 0.7\sqrt{\frac{8k\left(t_{eff} + \frac{t_m}{\varepsilon_{Si_3N_4}}\right)^3}{27\varepsilon_0 2\pi a^2}} \tag{14}$$

where k is the spring constant of the device:

$$k = \frac{192\pi D}{a^2} \tag{15}$$

From (14), device C has the highest pull-in voltage, of about 58 V, therefore, a DC bias voltage of either 170 V or −170 V was chosen to pre-charge the CMUTs. The charging time was set to 300 s.

D. FITTING PROCESS OVERVIEW

The fitting process was used to derive relevant parameters (i.e., σ, ρ and r_{charge}) by comparing the semi-analytical reduced order model (ROM) introduced in Section II to the measurement results. However, to avoid overfitting the ROM with all the measurement results, the ROM was sequentially tuned by feeding it with limited information and checking it against the measurement results.

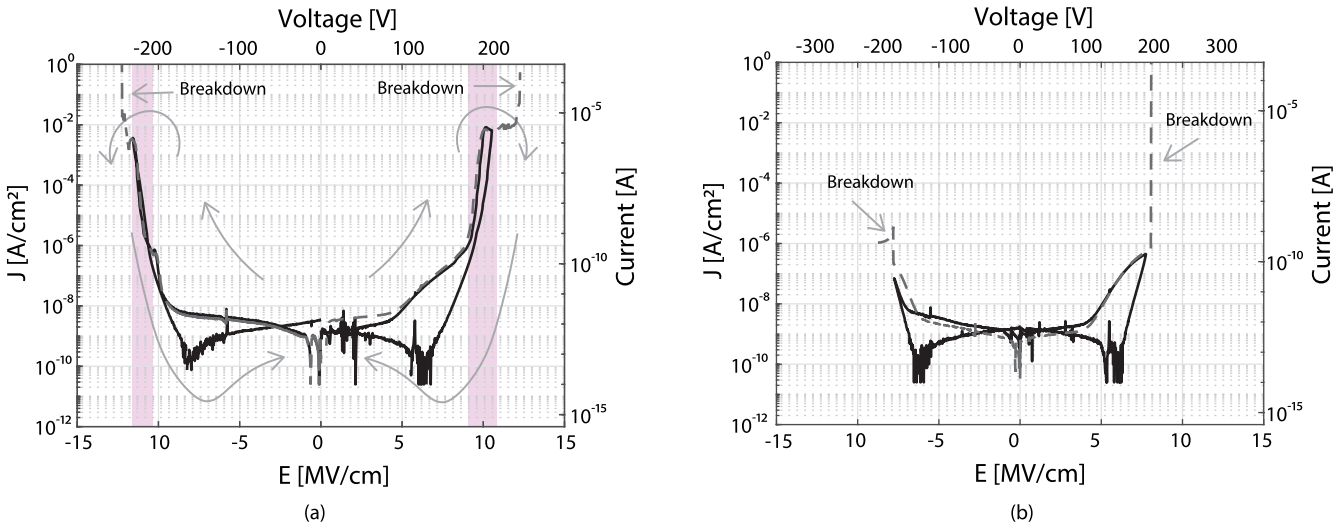

FIGURE 4. Example of I-V curves measured on the test capacitors. (a) layer stack A and (b) reference capacitor without Al_2O_3 layer. Left and bottom axes indicate the current density at a specific electric field, while the top and right axes indicate the voltage that needs to be applied to obtain the corresponding electric field. Direction arrows in a) indicate the direction of the voltage sweep and dashed lines indicate the measurement done to determine the breakdown voltage. Pink shaded area indicates the region of fast charging.

The fitting process of the ROM to the measurement result is as follows. First, the ROM is implemented in MATLAB with the membrane dynamics equation (11), layer stack, membrane geometry, and gap height. Secondly, using the membrane profile measured at 0 V, the uniform biaxial residual stress τ is tuned so that the membrane profile matches the measurement result. This serves as the baseline model of the CMUT with no charging. Then, the pull-in and snap-out voltages are predicted with the ROM and compared to the fast C-V curve measurements (5). Furthermore, the collapse diameter and C-V curve are compared with the measurement results to determine the surface charge and the volume charge.

IV. CHARACTERIZATION RESULTS

A. I-V MEASUREMENTS

The result of the I-V measurement on the capacitor variant A is shown in Fig. 4(a). For variants B to D, the results can be found in the supplementary Fig. S1. In addition, the measurement that was made on a reference capacitor with only SiO_2 as the dielectric material (EOT = 200 nm) is shown in Fig. 4(b). In both 4(a) and (b), a small leakage current of several nA cm^{-2}, independent of the electric field, is observed up to 4 to 5 MV cm^{-1} and, above this value, the current density gradually increases until around 7-8 MV cm^{-1}. When the electrical field is further increased above 7 to 8 MV cm^{-1}, the dielectric of the capacitor with only SiO_2 breaks down, as shown by the dashed line in Fig. 4(b). On the other hand, the current in the capacitors with the Al_2O_3 layer sharply rises (shaded region in Fig. 4(a)) before the hard breakdown, which occurs at electric fields in the order of 10-12 MV cm^{-1}. The shaded region indicates fast charging and is not present in the capacitor with only SiO_2 as dielectric. In the past, CMUTs with only SiO_2 as dielectric did not show noticeable charging. Therefore, we can infer that in order to trap charge, the material should show a region of fast charging. In addition, comparing the voltage used to charge the different CMUT variants, only for devices A to C the voltage lies in the shaded region. The effect of this difference on the amount of trapped charge will be discussed in Section IV-C.

B. FITTING THE MODEL WITH DHM MEASUREMENTS

Fig. 5(a) shows the membrane profile of variant A when the bias voltage was swept from 0 V to 120 V on a pristine CMUT device. From this figure, it can be seen that variant A has a pull-in voltage between 30 V to 40 V. The DHM measurements for variants B to D can be found in supplementary Fig. S2. In Fig. 5(a), the initial displacement at 0 V is caused by the atmospheric pressure and the uniform biaxial residual stress that was modeled in Section II.

In this section, the measurements and the simulation of the membrane profile at 0 V was compared for each variant to tune uniform biaxial residual stress parameter (τ). In Fig. 5(b) the dashed line shows the membrane profile at 0 V for all variants. For devices A and B, the center displacement of the membrane is about 200 nm, while for devices C and D, it is in the order of 100 nm. The τ is tuned such that the simulated membrane profile (solid line) matches the four variants (dashed line) as much as possible. The tuning process resulted in a negative stress in the order of several hundred of MPa (i.e. A:−650 MPa, B:−550 MPa, C:−650 MPa, D:−200 MPa). These values are large and cannot be fully explained by the stress resulting from the fabrication. Thus, it should be recognized that this stress value is also compensating for the subtle non-idealities within the model. Such

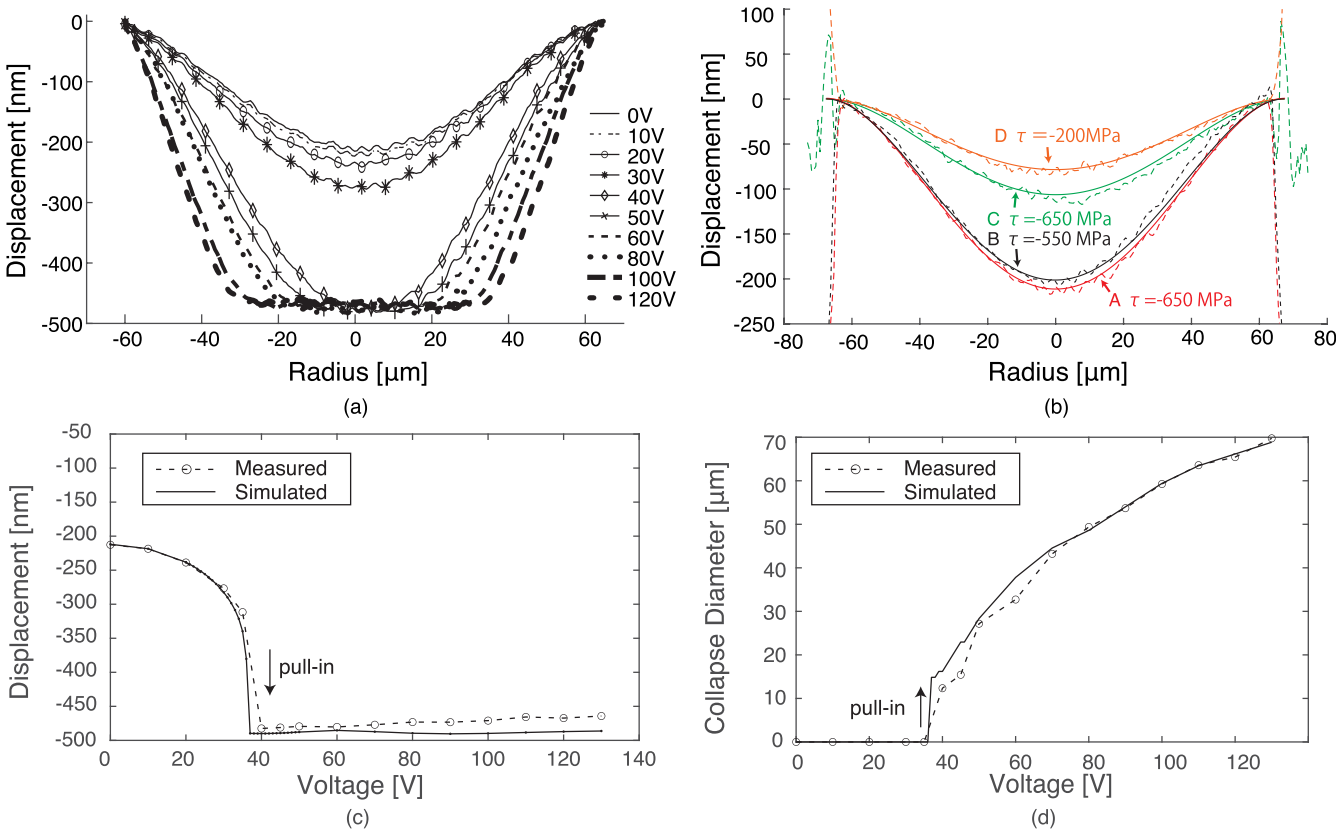

FIGURE 5. (a) Measurement result of the membrane profile for variant A. (b) Tuning result of the membrane profile after fitting. The dashed line is the simulation result and the measurement result is in the solid line. Comparison of the simulation result and the measurement result for variant A regarding the (c) center displacement and the (d) collapse diameter.

non-idealites can arise from the existence of the six plugging areas around the CMUT cell which will have some repercussions on the axisymmetric assumption of the model or the perfectly clamped assumption along the rim of the CMUT membrane.

After the tuning process, it can be seen that the measurement results and the simulation results are in good agreement. Fig. 5(c) and (d) is a comparison between the simulation result and the measurement result for variant A regarding the center displacement and the collapse diameter when different external voltages are applied. The comparison of the simulation results and the measurement results for the other CMUT variants can be found in supplementary Fig. S4 and Fig. S5.

C. FAST C-V MEASUREMENT

After being charged, the C-V curve of the CMUTs was measured. A unipolar sweeping protocol was used to keep the same polarity while charging and measuring. In addition, a bipolar sweep was done on a pristine device as a reference. In Fig. 6, the fast C-V measurement results are shown for the four variants. The solid blue line is the C-V curve of a pristine element, obtained with a bipolar sweep, which is symmetric with respect to 0 V for all the devices. The solid pink line represents the positive unipolar sweep, while the solid black line represents the negative unipolar sweep for a CMUT element charged with positive and negative polarity, respectively. In Fig. 6, devices A and B show the most significant shifts in the C-V curves with respect to the uncharged element. The C-V curves for A and B show that the CMUT elements are in collapse at 0 V bias and that around 40 V must be applied to bring them out of collapse. On the other hand, Fig. 6(c-d) shows that the amount of charge stored in devices C and D, which is proportional to the shift in the C-V curve, is not sufficient to keep the device in collapse. Since their thicker membrane and effective dielectric thickness require a larger voltage to bring the membrane into collapse, a higher amount of charge, compared to devices A and B, must be stored to keep the membrane in collapse.

As mentioned earlier, the C-V curve can shift either to the left or to the right with respect to the symmetrical reference curve, depending on the type of charge. However, assuming that no injection of holes can occur in the Al_2O_3 layer, the only possible explanation for the shift of the C-V curve to the right is that there is a downward polarization. Thus, these results indicate the polarization behavior of the Al_2O_3 layer. Ferroelectric-like behavior such as this was reported by Peng et al. [28], who associated this effect with oxygen vacancies that move due to the external electric field.

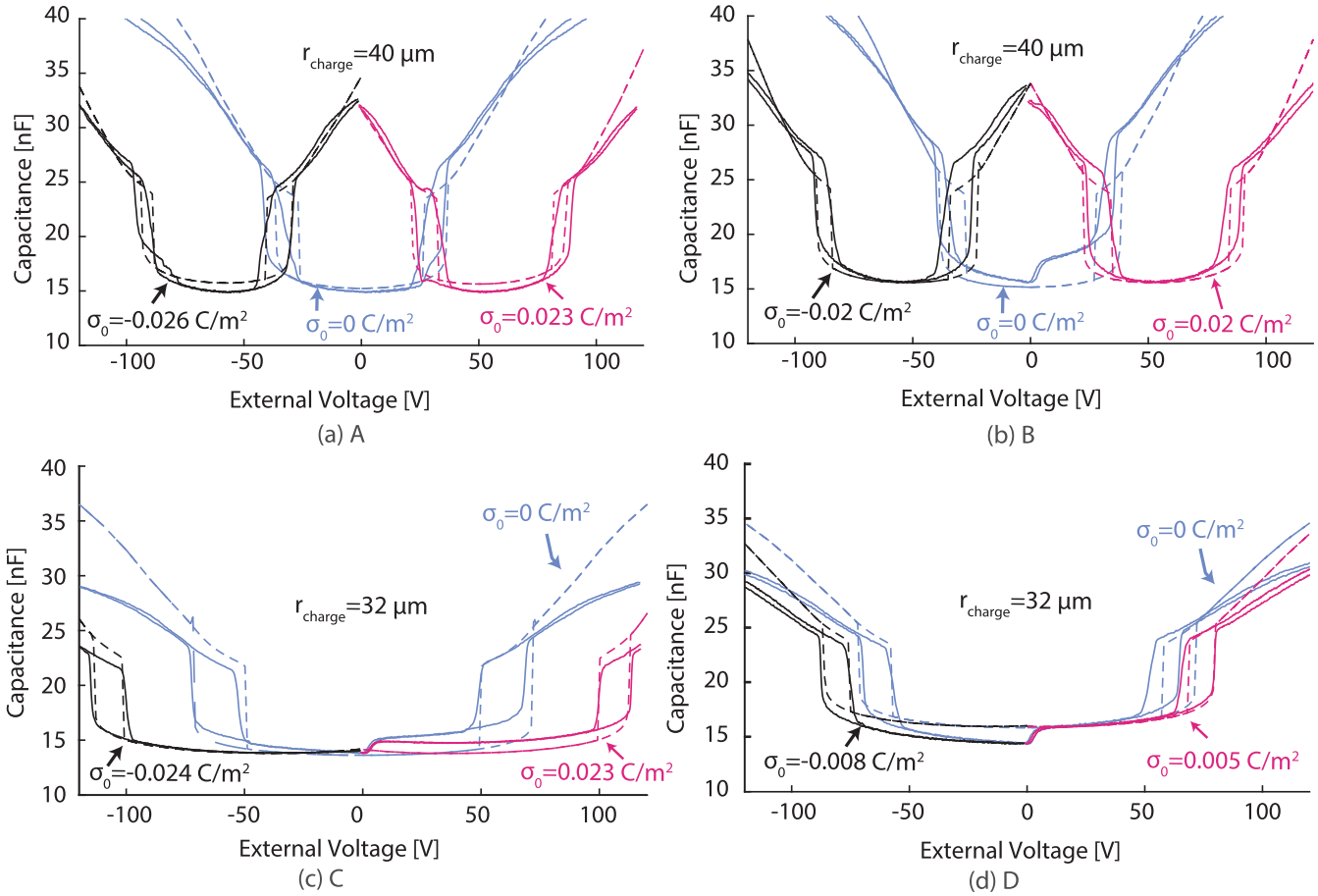

FIGURE 6. C-V curves of the four CMUT devices. Solid lines represent the measured values, while dashed lines represent the value fitted with the model. The blue line is the bipolar sweep done on a pristine device, the pink line is the positive unipolar sweep for a device positively charged and the black line is the negative unipolar sweep for a device negatively charged. (a) device A, (b) device B, (c) device C, (d) device D.

Additionally, the shift of the C-V curve to the left or to the right is nearly the same for all CMUTs. This shows that the polarization behavior of the Al_2O_3 layer is dominant compared to the fixed volume electron charges, which tend to pull the C-V curve only to the left. Thus, in the consecutive process of fitting the C-V curve, only the polarization is taken into account, and the fixed volume charges are ignored by setting $\rho_m = 0\,\mathrm{C\,m^{-2}}$.

Fig. 6 also shows the simulated C-V curve for all variants with a dashed line on top of the corresponding measurement result. The value of the capacitance is simulated from the membrane profile and does not include the membrane's transient movement, which is typically referred to as mechanical capacitance. In addition, the collapse radius at 170 V is simulated and used for the charge radius in each variant (i.e., for A and B: $r_{charge} = 40\,\mu\mathrm{m}$ and for C and D: $r_{charge} = 32\,\mu\mathrm{m}$. Then, the polarizing surface charge σ is tuned either to the positive or to the negative to fit the measured C-V curve. The required surface charge for each variant is also shown in Fig. 6. For A, B, and C, the amount of charge is nearly $0.02\,\mathrm{C\,m^{-2}}$, while for D, is significantly lower, approximately $0.0052\,\mathrm{C\,m^{-2}}$. This is because, during the charging process of device D, the electrical field across the device was lower due to the thicker insulation layer between the top and bottom electrodes. In addition, the voltage used to charge device D does not lie in the region of fast charging and polarization (Fig. 4), while this is the case for the other types of devices. This suggests that, in order to trap enough charge to obtain a collapse-mode device, the charging voltage should be chosen among that region, which, for the devices used in this work, corresponds to electric fields above 7-8 $\mathrm{MV\,cm^{-1}}$. However, care should be taken to not choose a voltage too high to cause breakdown of the dielectric. The amount of trapped charge is similar to the maximum charge density that has been reported in literatures [29], [30] $0.016\,\mathrm{C\,m^{-2}}$. From this analysis, devices A and B are both good candidates for the pre-charged collapse mode CMUT because they both remained in collapse after the charging process. In addition, because device A charged slightly more than device B, the following experiments focus on device A.

V. PERFORMANCE RESULTS

A. TRANSMIT SENSITIVITY

The bandwidth of the pre-charged collapse-mode CMUT (device A) was measured with an impulse response measurement in water and compared to a pristine CMUT with an

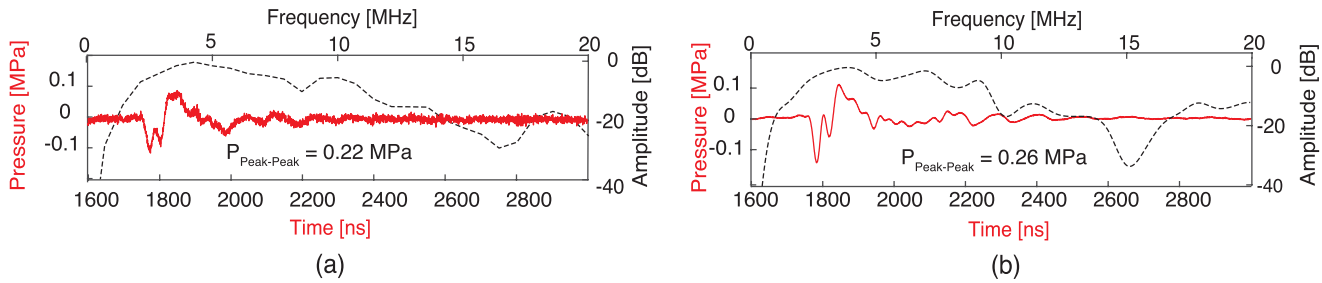

FIGURE 7. Transient pressure response (red) and frequency response (dashed line) measured with a hydrophone at 2.6 mm distance for (a) a CMUT charged with 170 V for several minutes. Impulse signal had a 25 V amplitude, with negative polarity and pulse width of 25 ns at full width half maximum; (b) a CMUT externally biased with 70 V. Impulse signal had a 25 V amplitude with positive polarity and a pulse width of 25 ns at full width half maximum.

external bias voltage. The measurement was conducted with 6 elements in parallel, each consisting of a row of 56 CMUT cells in parallel, accounting for a total width and height of the device of 0.84 mm and 7.56 mm respectively. The CMUT was pre-charged with a positive voltage of 170 V for several minutes. Then the device was immersed in water and an impulse signal with an amplitude of −25 V and a pulse width of 25 ns was applied. The acoustic response was measured with a fiber optic hydrophone (Precision Acoustic, UK) at 2.6 mm distance from the CMUT. Then the same experiment was repeated with a CMUT without stored charge. In this case, a bias voltage was externally applied from 60 V to 100 V in 10 V steps and the polarity of the impulse signal was flipped (i.e. positive impulse signal). The range of bias voltages used for this experiment is below the rapid charging state measured in Section IV-A and thus, the CMUT will not charge significantly, and a fair comparison can be made between a CMUT with and without charge. The result of the impulse response for all bias voltages can be seen in supplementary Fig. S5.

The result of the impulse response for the pre-charged CMUT is shown in Fig. 7(a). The peak-to-peak pressure was 0.22 MPa and the -6 dB bandwidth was 113 % with a center frequency of 5.1 MHz. The transmit sensitivity was 8.8 kPa V^{-1}. In comparison, the impulse response for the CMUT with an external bias voltage of 70 V is shown in Fig. 7(b). The peak-to-peak pressure was 0.26 MPa and the -6 dB bandwidth was 117 % with a center frequency of 5.0 MHz. The transmit sensitivity was 10.4 kPa V^{-1}. Thus, the acoustic performance of the pre-charged collapse-mode CMUT is nearly identical to a CMUT biased with 70 V.

B. RECEIVE SENSITIVITY

The receive sensitivity was measured by sending an ultrasound signal from a source and receiving it with the pre-charged collapse-mode CMUT. The schematic of the experimental setup is shown in Fig. 8(a) and a picture of the setup is shown in Fig. 8(b). In this experiment, ultrasound was generated by a transmitter (TX) CMUT (5 mm × 12 mm) with a frequency of 2 MHz generating a peak to peak pressure up to 0.6 MPa immediately in front of the receiver (RX) pre-charged CMUT. The RX had 8 CMUT elements in parallel, each consisting of a row of 56 CMUT cells in parallel, which resulted in a surface area of 7.56 mm × 0.95 mm. The distance between the TX and RX was 6 cm which was chosen such that the ultrasound hits the pre-charged collapse-mode CMUT array with a plane wave. This guarantees that all the CMUT cells operate in-phase, with the same voltage. To avoid standing wave formation between the TX and the RX, the ultrasound was sent in 10 cycles at 1 kHz pulse repetition frequency. Prior to the experiment, the electrical capacitance of the CMUT was measured to be 640 pF. The output of RX was connected to an adjustable impedance matching block on the same PCB as shown in Fig. 8(a). This block is composed of several inductors and resistors that can be manually connected with mechanical switches to compensate the electrical capacitance of the CMUT. The alignment of RX with respect to TX was adjusted by positioning the RX such that the maximum output voltage was achieved in an open circuit condition.

First, the output voltage was measured at the RX in open circuit condition for three different incident pressure values (Fig. 8(c) the line with circle markers). Then the inductive load was tuned to maximize the output voltage in order to compensate the electrical capacitance in the CMUT (Fig. 8(c) the line with triangle markers). This matched condition occurred at 10 μH which is in good agreement with the analytically calculated value of $L_{match} = 9.89\ \mu H$, according to $L_{match} = \frac{1}{(2\pi f_{res})^2 \cdot C_e}$ ($\because C_e = 640$ pF, $f_{res} = 2$ MHz). Finally, the matching resistor load was adjusted to $R_{load} = 360\,\Omega$ to achieve maximum power transfer (Fig. 8(c) the line with square markers). In this matched condition, the efficiency of the CMUT, defined from the plane immediately in front of the RX CMUT to the resistive load, was calculated for the three pressure values as shown in Fig. 8(d). From this figure, it can be seen that the efficiency at 0.18 MPa peak to peak is 45 % and decreases to 20 % at 0.6 MPa peak to peak due to non-linear effects. By linearly fitting the points in Fig. 8(c) the open circuit receive sensitivity is computed resulting in 13.1 V MPa^{-1}. The maximum power instantaneously harvested at the load was 47 mW when 0.6 MPa peak to peak pressure was applied. The coupling coefficient kt^2 of

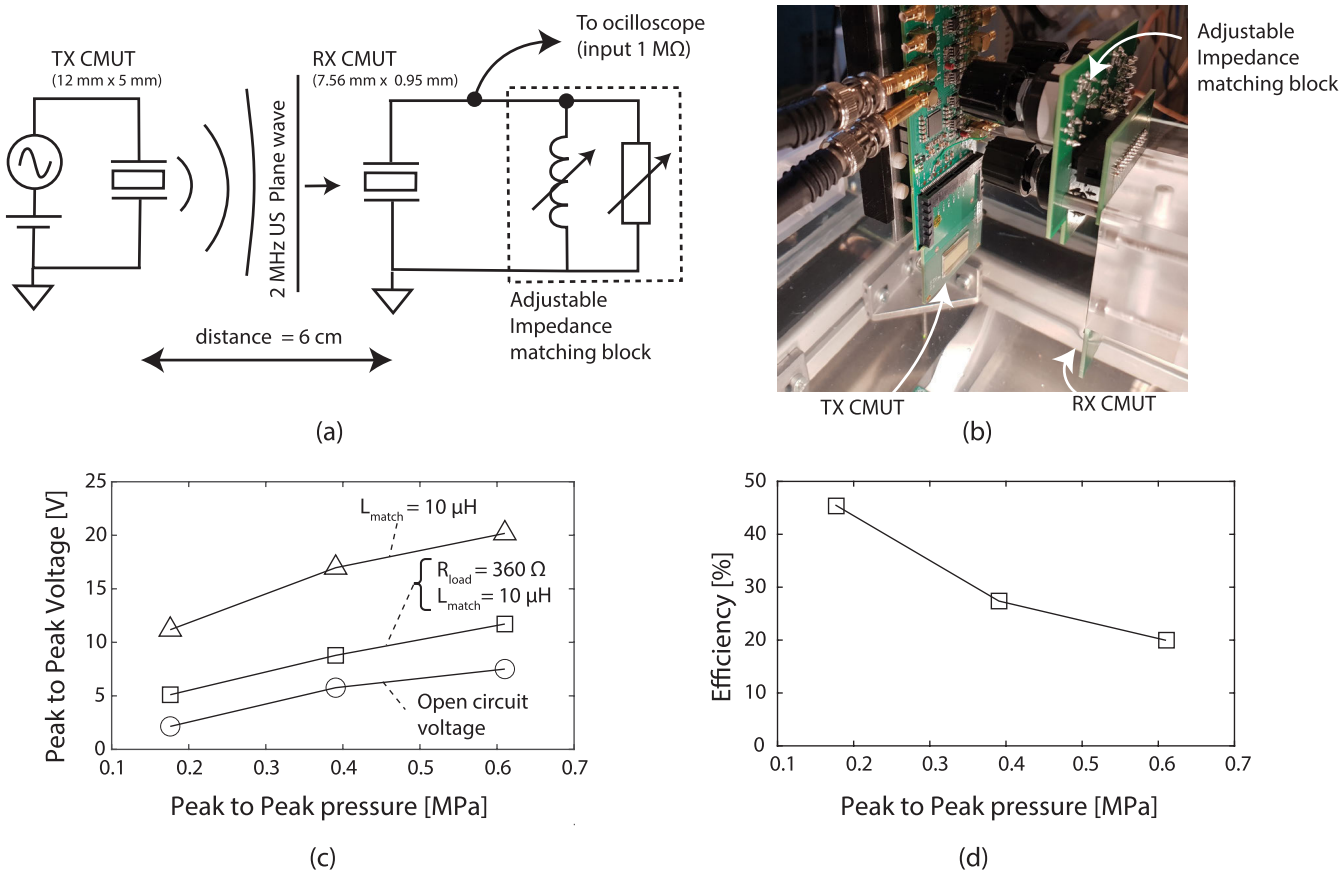

FIGURE 8. Power transfer experiments. (a) Schematic diagram of the setup (b) Picture of the experimental setup. (c) Output voltage measured at the receiver for varying loading conditions and (d) efficiency measured for matched load condition (R_{load} = 360 Ω and L_{match} = 10 μH). Both figures are plotted with respect to the incident peak to peak pressure.

the pre-charged collapse-mode CMUT was also calculated for a few pre-charged samples, resulting in about 0.7. In the supplementary Table S1, this result is compared to the results achieved by other groups, showing that its performance is comparable to PZT. In addition, the transmit sensitivity of our pre-charged collapse-mode CMUTs is in line with the characteristic values of other micromachined transducer technologies [8], and in terms of receive sensitivity the performance is in the top range or above other technologies.

C. RELATIONSHIP BETWEEN CHARGING PARAMETERS AND STORED CHARGE

With the objective to charge the CMUT as much as possible, several combinations of charging parameters (i.e., charging time, temperature, voltage, and polarity) have been investigated. The resonance frequency extracted from the air-coupled impedance measurement of a collapse-mode CMUT was used as a representative parameter indicating to what extent the CMUT was charged [24], [31]. Furthermore, the fast C-V curve measurement was not used because it was not sensitive enough to detect the subtle changes caused by the different charging parameters that were tested. The tested charging times were between 60 s and 600 s and the

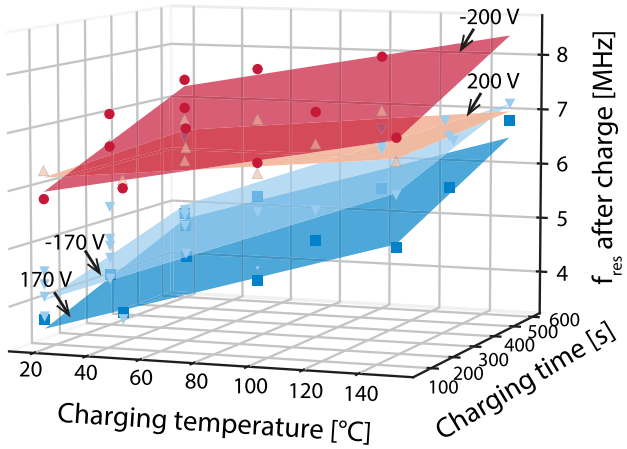

FIGURE 9. Effect of different charging parameters on the after charging resonance frequency of the CMUT device with layer stack A.

temperature of the sample during charging was varied between 20 °C and 150 °C. Two charging voltages were tested which were 170 V and 200 V, both with a positive and negative polarity. Fig. 9 shows the results of the experiment.

In this figure, a plane was fitted to the experimental results for each voltage and polarity, showing that a higher resonance frequency, therefore more charge, is stored by applying the charging voltage to the CMUT for a longer time and at a higher temperature. The increase in the amount of stored charge at higher temperatures is a known phenomenon in the field of device reliability [32], [33], [34]. The charging current is a thermally activated phenomenon, and combined with the decrease of the spring constant at elevated temperature, results in the acceleration of the charging process [35]. In addition, comparing the effect of the charging polarity for the same charging voltage, using a negative polarity results in a higher resonance frequency. This is because the effect of surface charge, which is the dominating mechanism, is combined with the effect of the volume charges, while for the positive polarity, the effect of the surface charges is attenuated by the opposing effect of the volume charges, as qualitatively explained in Section II-B. Furthermore, charging the device for a longer time results in a higher amount of charge stored in the device. To summarize, charging the device for a longer time, at a higher temperature, at a higher voltage, with a negative polarity result in a higher amount of stored charge. These relationships can be used to achieve faster and more efficient charging of the CMUTs.

D. LIFETIME ESTIMATION

In the prospect of the commercialization of the device, it is important to know how long the trapped charges are retained in the charging layer. To estimate the lifetime of the devices at different operating temperatures, Accelerated Lifetime Tests (ALT) have been performed on devices of type A with temperature as an accelerating factor. The failure time of the CMUTs can be fitted with the Arrhenius relation:

$$\text{lifetime}(T) = A \cdot \exp\left(\frac{\mathrm{E_A}}{\mathrm{k_B} \cdot \mathrm{T}}\right) \tag{16}$$

where $\mathrm{E_A}$ is the activation energy of the discharge process and $\mathrm{k_B}$ is the Boltzmann's constant $8.617 \times 10^{-5}\,\mathrm{eV\,K^{-1}}$. A is a constant that depends on the device geometry, size, test method and other factors, and can be estimated from the test data. Pristine CMUTs were charged with several combinations of parameters and after charging they were brought at the designated test temperature. Most of the devices were charged at room temperature, while a few tests were performed on devices charged at higher temperatures to confirm the result that are shown in Fig. 9. The test temperatures were between 100 °C and 150 °C, and the failure time of the devices was evaluated measuring the impedance at constant time intervals. The impedance spectrum of an air-coupled CMUT after charging shows a resonance peak at around 6 MHz (high frequency), which indicates that the CMUT cells are in collapse (Fig. 10). When the membrane of some of the CMUTs cells goes out of collapse, the equivalent capacitance of the device decreases (impedance spectrum shifts upwards), and a second resonance peak appears at a much lower frequency, at around 1.5 MHz, which corresponds to

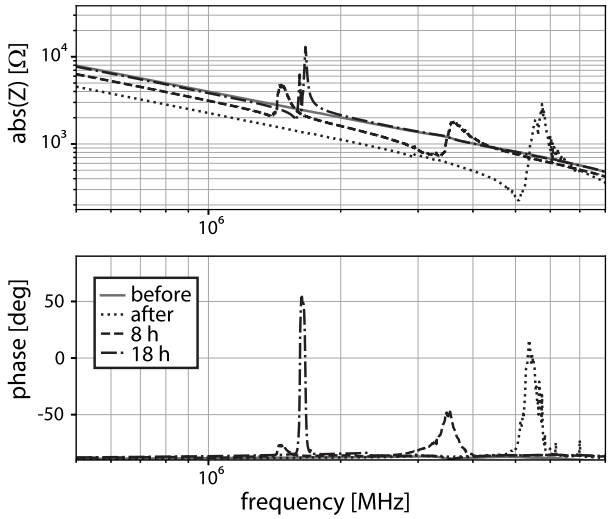

FIGURE 10. Example of air-coupled impedance spectrum of a CMUT device type A, measured at different points in time during ALT at high temperature. Only a few measured points are reported here for clarity.

the non-collapse mode of operation of the CMUT. When a cell of a pre-charged CMUT goes out of collapse, it is defined as failed because it cannot harvest ultrasound power in this state. The height of the resonance peaks at both high and low frequency changes over time due to the discharging and subsequent going out of collapse of the CMUT cells. During some of the lifetime tests, the shape of the cells in the element under test was examined with the DHM, and we observed that the height of the two peaks in the phase plot of the impedance spectrum (bottom plot of Fig. 10) correlates to the number of CMUT cells in collapse and non-collapse. The point in time at which the height of the peak at the lower frequency is larger than the height of the peak at high frequency is when more than half of the CMUT cells are out of collapse, which is defined as the failure time of the device.

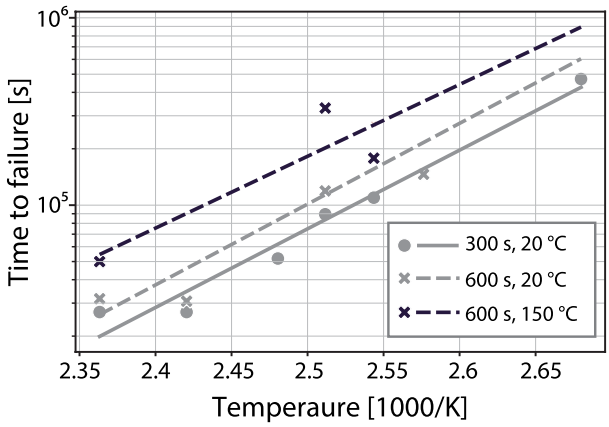

FIGURE 11. Fitting of the ALT results with the Arrhenius relation to predict lifetime of the devices charged at different temperatures.

In Fig. 11, the failure times obtained from some preliminary ALT tests have been fitted with the Arrhenius

relation (16). The results show that the lifetime of the devices increases when they are charged for a longer time and, extrapolating the lifetime at lower temperatures, at the minimum they have a lifetime of more than 2.5 years at body temperature (37 °C). In addition, the lifetime of a few samples charged at 150 °C showed an increase of about 50 % compared to devices charged at room temperature. Therefore, these results confirm that charging the CMUTs at higher temperature and for a longer time increases the lifetime. Although the ALT conditions used in this work may have accelerated the failure mechanisms as they occur in actual operation conditions, and more results are necessary to fully assess their lifetime, these results show the potential of these devices for a variety of applications, including in-body ultrasound power transfer and harvesting.

VI. CONCLUSION

In this paper, pre-charged collapse-mode CMUTs were studied through modeling and characterization of four device variants (A, B, C and D) with an Al_2O_3 layer between the top and bottom electrodes. To study their charging behavior, a semi-analytic reduced order model was developed following the approach of [22]. The model includes the built-in charging layer as an additional force term.

The charging behavior was first characterized in detail using I-V curves of test capacitors, that have the same layer stack as the CMUT, but without the vacuum gap. These I-V curves showed a region of fast charging and polarization before the hard breakdown, that was not present in the reference capacitor that only had SiO_2 as the dielectric material, thus indicating that charges are trapped within the CMUT because of the Al_2O_3 layer. In addition, it was found that to obtain pre-charged collapse-mode CMUTs the charging voltage needs to be in the range of values in the region of fast charging and polarization.

By fitting this model to the fast C-V curve measurement of the pre-charged collapse-mode CMUTs, it was shown that the Al_2O_3 layer has a polarizable behavior that can be controlled by the polarity of the charging voltage. Moreover, the amount of charge stored in each of the CMUT variant can be calculated from the model, resulting in a maximum surface charge density of $\sigma_0 = 0.026\,\mathrm{C\,m^{-2}}$ for variant A.

This device was then characterized with transmit and receive sensitivity measurements in water, showing a performance in line with biased CMUTs, with bandwidth and efficiency of the power harvesting were in line with values obtained by other groups. Finally, the amount of stored charge was maximized for variant A by testing additional charging parameters. It was found that charging the CMUTs at a higher temperature, for a longer time and with a higher voltage resulted in a larger amount of trapped charge. These CMUTs also showed a charge retention of 2.5 years at body temperature, making these devices promising candidates for applications requiring, among others, biocompatibility and manufacturing scalability.

APPENDIX

See Table 2.

TABLE 2. Summary of the symbols used in this work.

Symbol	Description
$\mathrm{t_m}$	Thickness of the top membrane
ρ_{tp}	Mass density of the top membrane
$\mathrm{t_g}$	Height of the vacuum gap
a	Membrane radius
r	Radial coordinate
$w(r)$	Displacement of the membrane along the radial direction
D	Flexual rigidity of the top membrane
$V(t)$	External voltage applied to the top membrane
σ_m	Standard deviation of the combined surface roughness
$\mathrm{H_{ab}}$	Indentation hardness
τ	Uniform biaxial residual stress
$\mathrm{t_{eff}}$	Effective gap height
t_i	Dielectric layer thickness, where $i = 1, 2, 3, 4$
$\varepsilon_{Al_2O_3}$	Relative permittivity of Al_2O_3
ε_{SiO_2}	Relative permittivity of SiO_2
$\rho(r)$	Volume charge along the radial direction $[\mathrm{C/m^3}]$
$\sigma(r)$	Surface charge along the radial direction $[\mathrm{C/m^2}]$
$x_1(r)$	Equivalent vacuum height
$\mathrm{x_2}$	Equivalent dielectric thickness
$\mathrm{t_3}^*$	Equivalent oxide thickness of Al_2O_3 layer
$P_e(r)$	Electrostatic pressure
$V_{eff}(r)$	Effective voltage due to the built-in charge
$s(r)$	Gap height along the radial direction
$\sigma_1(r)$	Combined contribution of surface and volume charge
$\mathrm{P_{atmos}}$	Atmospheric pressure
σ_0	Surface charge density
ρ_0	Volume charge density
r_{charge}	Contact radius during charging
$\mathrm{V_{pi}}$	Pull-in voltage
k	Spring constant
kt^2	Electromechanical coupling coefficient

ACKNOWLEDGMENT

The authors acknowledge the contribution of researchers working at Philips Research and at Philips Engineering Solutions for the fabrication of the CMUTs and for their help in performing some of the measurements. Martin Pekař for helping with the modeling, Eugene Timmering for the fabrication of the devices, Peter Loebl and Peter Blanken for the constructive discussions. *(Marta Saccher and Shinnosuke Kawasaki contributed equally to this work.)*

REFERENCES

[1] T. L. Szabo, *Diagnostic Ultrasound Imaging: Inside Out*. Amsterdam, The Netherlands: Elsevier, 2004.

[2] J. Joseph, B. Ma, and B. T. Khuri-Yakub, "Applications of capacitive micromachined ultrasonic transducers: A comprehensive review," *IEEE Trans. Ultrason., Ferroelectr., Freq. Control*, vol. 69, no. 2, pp. 456–467, Feb. 2022.

[3] D. M. Becker, C. A. Tafoya, S. L. Becker, G. H. Kruger, M. J. Tafoya, and T. K. Becker, "The use of portable ultrasound devices in low- and middle-income countries: A systematic review of the literature," *Tropical Med. Int. Health*, vol. 21, no. 3, pp. 294–311, Mar. 2016.

[4] Y. Baribeau et al., "Handheld point-of-care ultrasound probes: The new generation of POCUS," *J. Cardiothoracic Vascular Anesthesia*, vol. 34, no. 11, pp. 3139–3145, Nov. 2020.

[5] D. K. Piech et al., "A wireless millimetre-scale implantable neural stimulator with ultrasonically powered bidirectional communication," *Nature Biomed. Eng.*, vol. 4, no. 2, pp. 207–222, 2020.

[6] G. L. Barbruni, P. M. Ros, D. Demarchi, S. Carrara, and D. Ghezzi, "Miniaturised wireless power transfer systems for neurostimulation: A review," *IEEE Trans. Biomed. Circuits Syst.*, vol. 14, no. 6, pp. 1160–1178, Dec. 2020.

[7] S. Kawasaki, Y. Westhoek, I. Subramaniam, M. Saccher, and R. Dekker, "Pre-charged collapse-mode capacitive micromachined ultrasonic transducer (CMUT) for broadband ultrasound power transfer," in *Proc. IEEE Wireless Power Transf. Conf. (WPTC)*, Jun. 2021, pp. 1–4.

[8] C. Visser et al., "A European MEMS ultrasound benchmark," Helath.E Lighthouse, White Paper, 2021. [Online]. Available: https://www.s2e2.fr/wp-content/uploads/2022/03/CMUT-PMUT-Benchmark-Technical-Whitepaper.pdf

[9] H. Martinussen, A. Aksnes, and H. E. Engan, "Investigation of charge diffusion in CMUTs using optical interferometry," in *Proc. Ultrason. Symp.*, Nov. 2008, pp. 1218–1221.

[10] K. Midtbo and A. Ronnekleiv, "Analysis of charge effects in high frequency CMUTs," in *Proc. Ultrason. Symp.*, Nov. 2008, pp. 379–382.

[11] L. L. P. Wong, S. Na, A. I. H. Chen, and J. T. W. Yeow, "A novel method for measuring dielectric charging of CMUT arrays," in *Proc. IEEE Int. Ultrason. Symp.*, Sep. 2014, pp. 185–188.

[12] J. A. Kittl et al., "High-K dielectrics for future generation memory devices (invited paper)," *Microelectron. Eng.*, vol. 86, nos. 7–9, pp. 1789–1795, Jul. 2009.

[13] W. Xu and Y. Ni, *Memory Characteristics and Mechanisms in Transistor-Based Memories*. Amsterdam, The Netherlands: Elsevier, 2020, pp. 53–73.

[14] C. Zhao, C. Zhao, S. Taylor, and P. Chalker, "Review on non-volatile memory with high-K dielectrics: Flash for generation beyond 32 nm," *Materials*, vol. 7, no. 7, pp. 5117–5145, Jul. 2014.

[15] W. Y. Choi, C. H. Lee, Y. H. Kim, and K. K. Park, "Comparison of Si_3N_4–SiO_2 and SiO_2 insulation layer for zero-bias CMUT operation using dielectric charging effects," *IEEE Trans. Ultrason., Ferroelectr., Freq. Control*, vol. 67, no. 4, pp. 879–882, Apr. 2020.

[16] F.-Y. Lin, W.-C. Tian, and P.-C. Li, "CMOS-based capacitive micromachined ultrasonic transducers operating without external DC bias," in *Proc. IEEE Int. Ultrason. Symp. (IUS)*, Jul. 2013, pp. 1412–1415.

[17] M.-C. Ho, M. Kupnik, K. K. Park, and B. T. Khuri-Yakub, "Long-term measurement results of pre-charged CMUTs with zero external bias operation," in *Proc. IEEE Int. Ultrason. Symp.*, Oct. 2012, pp. 89–92.

[18] K. K. Park, M. Kupnik, H. J. Lee, O. Oralkan, and B. T. Khuri-Yakub, "Zero-bias resonant sensor with an oxide-nitride layer as charge trap," in *Proc. IEEE Sensors*, Nov. 2010, pp. 1024–1028.

[19] A. Kshirsagar, A. Sampaleanu, R. Chee, W. Moussa, and R. J. Zemp, "Pre-charged CMUTs with efficient low-bias voltage operation for medical applications," in *Proc. IEEE Int. Ultrason. Symp. (IUS)*, Jul. 2013, pp. 1728–1730.

[20] G. D. Wilk, R. M. Wallace, and J. Anthony, "High-K gate dielectrics: Current status and materials properties considerations," *J. Appl. Phys.*, vol. 89, no. 10, pp. 5243–5275, 2001.

[21] H. Köymen, A. Atalar, S. Güler, I. Köymen, A. S. Tasdelen, and A. Ünlügedik, "Unbiased charged circular CMUT microphone: Lumped-element modeling and performance," *IEEE Trans. Ultrason., Ferroelectr., Freq. Control*, vol. 65, no. 1, pp. 60–71, Jan. 2018.

[22] M. Pekař, S. H. M. van Nispen, R. H. B. Fey, S. Shulepov, N. Mihajlović, and H. Nijmeijer, "A fluid-coupled transmitting CMUT operated in collapse mode: Semi-analytic modeling and experiments," *Sens. Actuators A, Phys.*, vol. 267, pp. 474–484, Nov. 2017.

[23] G. M. Sessler, "Spatial depth and density of charge in electrets," *J. Appl. Phys.*, vol. 43, no. 2, pp. 408–411, Feb. 1972.

[24] M. Pekař, W. U. Dittmer, N. Mihajlović, G. van Soest, and N. de Jong, "Frequency tuning of collapse-mode capacitive micromachined ultrasonic transducer," *Ultrasonics*, vol. 74, pp. 144–152, Feb. 2017.

[25] G. W. Vogl and A. H. Nayfeh, "A reduced-order model for electrically actuated clamped circular plates," *J. Micromech. Microeng.*, vol. 15, no. 4, pp. 684–690, Apr. 2005.

[26] J. H. Klootwijk, P. Dirksen, M. Mulder, and E. M. L. Moonen, "Capacitive micromachine ultrasound transducer," U.S. Patent 9 132 693, Sep. 15, 2015.

[27] S. Olcum, M. N. Senlik, and A. Atalar, "Optimization of the gain-bandwidth product of capacitive micromachined ultrasonic transducers," *IEEE Trans. Ultrason., Ferroelectr., Freq. Control*, vol. 52, no. 12, pp. 2211–2219, Dec. 2005.

[28] Y. Peng et al., "Ferroelectric-like behavior originating from oxygen vacancy dipoles in amorphous film for non-volatile memory," *Nanosc. Res. Lett.*, vol. 15, no. 1, pp. 1–6, Dec. 2020.

[29] J. J. H. Gielis, B. Hoex, M. C. M. van de Sanden, and W. M. M. Kessels, "Negative charge and charging dynamics in Al_2O_3 films on Si characterized by second-harmonic generation," *J. Appl. Phys.*, vol. 104, no. 7, 2008, Art. no. 073701.

[30] X. Zhang, B.-W. Liu, Y. Zhao, C.-B. Li, and Y. Xia, "Influence of annealing temperature on passivation performance of thermal atomic layer deposition Al_2O_3 films," *Chin. Phys. B*, vol. 22, no. 12, Dec. 2013, Art. no. 127303.

[31] Ö. Oralkan et al., "Experimental characterization of collapse-mode CMUT operation," *IEEE Trans. Ultrason., Ferroelectr., Freq. Control*, vol. 53, no. 8, pp. 1513–1523, Aug. 2006.

[32] N. Tavassolian et al., "The effect of silicon nitride stoichiometry on charging mechanisms in RF-MEMS capacitive switches," *IEEE Trans. Microw. Theory Techn.*, vol. 57, no. 12, pp. 3518–3524, 2009.

[33] R. Daigler, G. Papaioannou, E. Papandreou, and J. Papapolymerou, "Effect of dielectric film thickness on dielectric charging of RF MEMS capacitive switches," in *IEEE MTT-S Int. Microw. Symp. Dig.*, Jun. 2008, pp. 1275–1278.

[34] R. Daigler, E. Papandre, N. Tavassolian, M. Koutsoureli, G. Papaioannou, and I. Papapolymerou, "Dependence of dielectric charging on film thickness and deposition conditions," in *Proc. Asia–Pacific Microw. Conf.*, Dec. 2008, pp. 1–4.

[35] X. Yuan, Z. Peng, J. C. M. Hwang, D. Forehand, and C. L. Goldsmith, "Acceleration of dielectric charging in RF MEMS capacitive switches," *IEEE Trans. Device Mater. Rel.*, vol. 6, no. 4, pp. 556–563, Dec. 2006.

MARTA SACCHER (Graduate Student Member, IEEE) received the B.Sc. degree in biomedical engineering from Polytechnic University of Milan, Italy, in 2017. In 2019, she obtained the M.Sc. degree (cum laude) in biomedical engineering from Delft University of Technology (TU Delft), the Netherlands and later joined the department of Biomedical Instrumentation and Signal Processing at Aarhus University, Denmark, as a postgraduate student. She is currently pursuing the Ph.D. degree at TU Delft in the Electronic Components, Technology and Materials group in the framework of the European project Moore4Medical, that aims to create an open technology platform for medical devices. She is currently based in Eindhoven, at Philips Research, where she is investigating the use of CMUTs for implantable medical devices for both power transfer and as a means of ultrasound modulation of the nervous system.

SHINNOSUKE KAWASAKI was born in Kanagwa, Japan, in March 1993. He received the Bachelor of Science (B.Sc.), in field of electrical engineering from the Tokyo Institute of Technology, Japan, in 2016. He completed the Master of Science (M.Sc.) degree in the field of Microelectronics from Delft University of Technology (TUDelft), in 2017 and then continued as a Ph.D. student at the Electronic Components, Technology Materials (ECTM) group in the Microelectronics Department also at TUDelft. He is also a Guest Researcher at Philips Research. His research interest lies in the area of collapse-mode capacitive micromachined ultrasonic transducers (CMUT) technology for various applications, such as, power harvesting, neurostimulation, and handheld ultrasound.

JOHAN H. KLOOTWIJK (Senior Member, IEEE) received the M.Sc. and Ph.D. degrees in electrical engineering from the University of Twente, Enschede, The Netherlands, in 1993 and 1997, respectively. Then, he joined Philips Research Laboratories, Eindhoven, where he has worked on a wide range of topics, a.o. wideband RF applications (a.o. Si, SiGe, and InP bipolar technologies), gas-sensors, thin EUV membranes (pellicles) for next generation lithography tools, and wearable MEMS-based ultrasound patches. In 2021, he was appointed as the Team-Lead at the Ultra-Sound Applications Team, Digital U.S. Solutions. He has authored or coauthored more than 80 scientific publications and conference contributions and holds more than 25 U.S. patents. He has been a Senior Lecturer on semiconductor devices at the CTT and T2Prof institutes, since 1999. He received the Best Paper Award for his contribution on the ESSDERC Conference in 2001 and the Best Poster Award on the NATO-ASI summer course on ALD in 1995. For part of his work, he received the Bronze Award for the "NXP Invention of the Year 2007" and the Bronze and Silver Invention Award in 2015 and 2020, respectively. He served as the Tutorial Chairman for the International Conference on Measurement and Teststructures (ICMTS) in 2002, 2008, and 2011; and the Technical Chairman in 2014.

ROB VAN SCHAIJK received the master's degree in applied physics from the Technical University of Eindhoven in 1995 and the Ph.D. degree in semiconductor physics from the University of Amsterdam in 1999. He joined Philips in the MEMS and Micro Devices department as a Principal Architect, in 2017. His main responsibility is MEMS process development in the Philips MEMS foundry with a focus on CMUT technology. With 20 years of experience in semiconductors, MEMS, and IC technology in different positions, from a Senior Scientist to the Research and Development Manager. Before joining Philips, he has been with Philips Research, Philips Semiconductors, NXP Semiconductors, and Imec, on topics in silicon processing, energy harvesting, and sensors for use in wireless sensor nodes.

RONALD DEKKER received the M.Sc. degree in electrical engineering from the Technical University of Eindhoven and the Ph.D. degree from the Technical University of Delft. He joined Philips Research in 1988, where he worked on the development of RF technologies for mobile communication. Since 2000, he has been focusing on the integration of complex electronic sensor functionality on the tip of the smallest minimal invasive instruments, such as catheters and guide-wires. In 2007, he was appointed as a part-time Professor at the Technical University of Delft, with a focus on organ-on-chip and bioelectronics medicines. Since 2013, he has been the initiator of a number of large European initiatives that all have in common the development of open technology platforms for electronic medical devices. In 2018, he initiated the ECSEL Joint Undertaking Health.E Lighthouse. He has published in leading journals and conferences and holds in excess of 70 patents.